Snežana S. Milićev

Associate Professor
University of Belgrade
Faculty of Mechanical Engineering

An Experimental Study
of the Influence of Spike
in Supersonic and Transonic Flows
Past a Hemispheric Body

Abstract: A strong shock wave during a supersonic flight of a blunt-nosed projectile increases the drag and aerodynamic heating considerably. A spike can be mounted on the nose of the projectile to reduce these effects. Apart from its very existence and its length, the spike's shape may also affect the aerodynamic characteristics of a blunt body. This paper presents the results of an experiment that analyzed the influence of the spike's shape on the aerodynamic forces and moments coefficients, and the location of the center of pressure, at supersonic and transonic flows past a model of a projectile with a hemispheric forebody. The experiment was carried out in a trisonic wind tunnel, for Mach numbers M=1.89 and M=1.03 and different angles of attack (0°-10°). Visualization of the experiments was performed by the schlieren method in the case of supersonic flow. It enables qualitative analysis of the airflow around the tested model without and with four different spikes. The conclusions are by the obtained values of the aerodynamic coefficients. The experiments show that a spike and its shape affect only the performance of the tested projectile during its supersonic flight. Besides, a spike does not affect or even slightly impairs the aerodynamic performance of the projectile during its transonic flight. The obtained results are applicable in broader contexts, e.g. for the design of an aircraft for supersonic flights.

Keywords hemispheric projectile, spike, supersonic flow, shock wave, angle of attack, aerodynamic coefficients, transonic flow.

1. INTRODUCTION

Although blunt bodies are aerodynamically unsuitable, such construction cannot be avoided sometimes. The hemispheric tip of a rocket allows the necessary equipment to be mounted in its front part. It may also be preferred for better heat distribution. It is well known that in the case of a supersonic flight of a blunt body, an extremely strong shock wave appears in front of the body, causing an intensive drag force. Moreover, there is a significant increase in both pressure and temperature near the stagnation point. A very simple idea to substantially reduce the drag force of a blunt body is to mount a spike on its fore-body [1-17]. In that way, the physics of the flow around the body changes completely. Instead of a strong shock wave, several weaker shocks appear then, causing the reduction of the drag force, aerodynamic heating of the body, the driving force, and consequently, the fuel consumption. How–ever, a spike can sometimes complicate the control of the body during its supersonic flight due to possible oscillations.

Many authors have treated the problem of the spike's influence on the supersonic flow around the blunt-nosed body experimentally. Chang [1, 2], as well as Krasnov and Koshevoy [3], made detailed surveys on this topic. More recently, Ahmed and Qin [4] gave a very detailed survey of the key studies of spiked bodies. Huang et al. [5] made a review of drag and heat flux reduction mechanisms induced by the spike mounted on the body in supersonic flows.

Many results have been obtained for bodies of revolution with flat and hemispheric noses. Mair [6] gave the results for such bodies with and without central spikes of different lengths, for Mach number $M = 1.96$ and Reynolds number $Re = 1.3 \cdot 10^5$ per cm. Hahn [7] presented the influence of the spike for $M = 3.3$. Bogdanoff and Vas [8] analyzed the influence of the spike on blunt bodies flying with hypersonic speeds $M \in [12,14]$. The axial spike was in the form of a cylinder with a conical nose of angle 11°. Mair [6] and Calarese and Hankey [9] investigated the conditions for the occurrence of oscillatory flow around the bodies with flat and hemispheric noses. They concluded that for bodies with hemispheric noses, the oscillatory flow does not appear.

The authors mostly focused on the influence of the spike's length on the aerodynamic characteristics of blunt bodies, for various angles of attack and Mach and Reynolds numbers. However, there is also an influence on its shape. In our previous papers, we compared the influence of spike shapes analyzing the drag and lift coefficients obtained in experiments, excluding the base

drag. Those results correspond to axisymmetric flow [10], flow at an angle of attack near to 2 degrees [11], and flow with angles of attack up to 10 degrees [12, 13]. Sahoo et al. [14] and Tembhurnikar et al. [15] numerically modeled the similar effect of the drag reduction by an intermediate aerodisk mounted on a sharp tip spike, compared with a sharp tip spike without a disk, for hemispheric fore-body. Ahmed and Qin [16] analyzed numerically the optimum size of an aerodisk that produced the largest drag reduction for a spiked hemispheric body at hypersonic flow, while Yadav and Guven [17] proposed a double-disk aerospike using results obtained with commercial software.

This paper attempts to complete the study of the influence of spike shapes mounted on a blunt body during its supersonic and transonic flights, by analyzing experimental results obtained in a wind tunnel. The measurements enabled a detailed review of aerodynamic characteristics of the cylindrical body with a hemispheric nose without and with four different spikes. In addition, visualization of the airflow in the supersonic domain, using the schlieren method, was completed by the measurements.

2. THE WIND TUNNEL FACILITY AND THE GEOMETRY OF THE TESTED MODELS

The wind tunnels at the Military Technical Institute (VTI) in Belgrade, Serbia, are being checked periodically, ensuring the measurement accuracy of calibration and other models [19-21]. Many results have been reported from these checks. Ocokoljic et al. [19] accomplished inter-facilities calibration using the standard AGARD-B model in subsonic airflow. Damljanovic et al. [20] obtained results for the same model in the transonic domain and compared them with the results from six relevant whirlwind tunnels for the same flow conditions. The same authors also analyzed the results for standard models obtained at non-standard conditions [21]. The regular testing of the standard calibration models ensures both the verification of the airfield parameters in the test sections and valid conditions of the wind tunnels instrumentation.

All the experiments were carried out in the trisonic indraft wind tunnel T-36 (Fig. 1) at the VTI. The experiments were performed using a model (actual projectile) and four different spikes, which were adapted for use in the wind tunnel. The tested model and the four spikes were made of steel, finished with high surface quality, and fabricated with 1% tolerance.

Figure 1. A photo of the trisonic indraft wind tunnel T-36

The model without a spike and with four different spike geometries was tested. The model is cylindrical with diameter $d = 27$ mm and length $L = 4.44d$, with a hemispheric fore-body, a conical tail with an angle of 9°, and with the basis diameter $d_b = 0.85d$. All the four tested spikes are of the same length $l_s = d$ and diameter $d_s = 0.17d$. Spike 1 is of the cylindrical body with a conical nose with an angle of 20°. Spike 2 and spike 3 are conical with the angles of 5° and 10°, respectively. The tips of these three spikes are rounded. Spike 4 is of the cylindrical body with a hemispheric nose. The tail of each tested spike is conical and twisted into the hemispheric nose of the model (Fig. 2). The technical drawings of the model and the spikes can be found in [13].
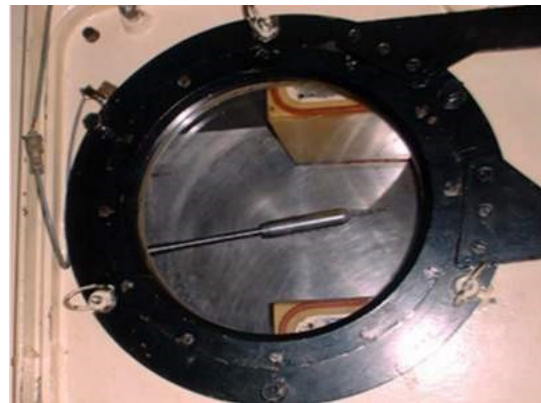

Figure 2. A photo of the tested model in the wind tunnel T-36

T-36 is a small open-wind facility with interrupted action. Its test section is 0.25 m × 0.25 m with a length 0.6 m. Two vacuum reservoirs with capacity $(485 + 820)$ m^3 and pressure $p = 0.1$ bar assure a measurement period (duration of a test) up to 60 s. For subsonic and transonic flows, the Mach number ranges from 0.2 to 1.1. For supersonic flows, there are four different fixed nozzles, which enable four fixed values of Mach number: $M_\infty \approx 1.56, 1.86, 2.46,$ and 3.24. Reynolds number can go up to 15×10^6 per meter.

Figure 3 shows a schematic view of the T-36 tunnel with its basic parts, marked with numbers.
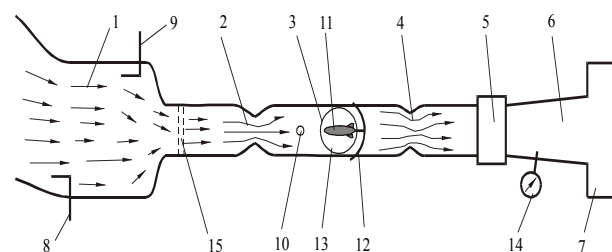

Figure 3. A schematic view of the trisonic indraft wind tunnel T-36

The measuring devices with the following expected accuracies were used during the measurements in the T-36 wind tunnel:

- Internal six-components strain gauge balance, multi-piece type: diameter 12 mm, normal force (F_n) capacity 200 N, axial force (F_a) capacity 40 N, pitching moment (M_p) capacity 4 Nm, accuracy 0.25% FS on individual components. The connection between the

model (11) and the balance was made by an octagonal pyramid (12), especially used for this type of balance.

- Differential pressure transducer measuring the difference between the stagnation pressure (p_0) in the silencing chamber (1) and the static pressure (p) in the test section (3) of the wind tunnel, type IHTM, with the range from 0 to 0.5bar and accuracy 0.029%.

- Differential pressure transducer (10) measuring basic pressure (p_b), type PDCR42, with the range from 0 to 0.35 bar and accuracy 0.06% FS.

- Absolute pressure transducer (9) measuring the stagnation pressure (p_a) in the silencing chamber, type IHTM, with the range from 0 to 1.75 bar, accuracy 0.027%.

- Absolute pressure transducer (14) measuring the pressure in the reservoir (7), type Kulite, with the range from 0 to 3.5 bar, accuracy 0.026%.

- Temperature sensor (8) measuring the stagnation temperature (T_0) in the silencing chamber, type RTD, accuracy 0.01°C.

- Potentiometer in the mount of the model, measuring the angle of attack (α), accuracy 0.01°.

- Data acquisition system NEFF 600, connected to a computer for control and data treatment, accuracy (0.02%+2μV).

- Schlieren system for visualization of the fluid flow field. A classic Teppler system was used, specially designed to meet high demands for quality and accuracy.

In addition, (2) and (4) are De Laval nozzles, (5) is a valve, (6) is a diffuser, (13) are the windows for visualization, and (15) are screens and honeycomb.

Mach number in the test section M, the air velocity u, density ρ, and dynamic pressure ($p_d=0.5\rho u^2$), may be calculated based on the measured values of the stagnation pressure p_0 and temperature T_0 in the silencing chamber and static pressure p in the test chamber, using the well-known equations of one-dimensional Gas dynamics [18]:

- The energy equation for an isoenergetic gas flow:

$$\frac{T_0}{T} = 1 + \frac{\kappa - 1}{2} M \,, \tag{1}$$

where $M=u/c$, $c = \sqrt{\kappa RT}$ is the speed of sound, κ is the ratio of specific heat, and R is the gas constant (for air κ=1.4 and R=287J/(kgK)).

- The relation between stagnation and static temperature and pressure for an isentropic gas flow:

$$\frac{p_0}{p} = \left(\frac{T_0}{T}\right)^{\frac{\kappa}{\kappa-1}}. \tag{2}$$

- The equation of state for an ideal gas:

$$\frac{p}{\rho} = RT \,. \tag{3}$$

The Sutherland relation is used for the calculation of dynamic viscosity:

$$\mu = \mu_* \left(\frac{T}{T_*}\right)^{1.5} \left(\frac{T_* + 110}{T + 110}\right), \tag{4}$$

where $\mu_* = 1.79 \cdot 10^{-5}$ Pas is the dynamic viscosity of air at temperature T_*=288K. If the diameter of the body d is the reference length, the Reynolds number is:

$$Re = \frac{ud}{\nu} \,, \tag{5}$$

where $\nu=\mu/\rho$ is kinematic viscosity.

During the wind tunnel tests, the air velocity vector lies in the vertical plane in which the model axis lies, so does the main vector, whereas the main moment is perpendicular to it. Because of that, the wind-tunnel balance, for different angles of attack α, measures only the axial force F_a, normal force F_n, and the pitching moment M_p. The aerodynamic coefficients of the tangential and normal forces are obtained by dividing them by the reference force value Ap_d:

$$c_a = \frac{F_t}{Ap_d}, \quad c_n = \frac{F_n}{Ap_d} \,. \tag{6}$$

The pitching moment coefficient is:

$$c_m = \frac{M_p}{dAp_d} \,, \tag{7}$$

where dAp_d is the reference moment value and $A=d^2\pi/4$ is the area of the cylindrical model's cross-section. The drag force c_d and lift force c_l coefficients can be calculated using c_t and c_n:

$$\begin{aligned} c_d &= c_a \cos\alpha + c_n \sin\alpha, \\ c_l &= c_n \cos\alpha - c_a \sin\alpha. \end{aligned} \tag{8}$$

The accuracy of the instruments that measured each quantity that defines the aerodynamic coefficients is given in the previous chapter. Taking it into account, the estimated accuracy of the coefficients is 0.035.

3. RESULTS, ANALYSIS, AND VALIDATION

The model without a spike and with four different spike geometries was tested in two cycles of measurements in a supersonic (M=1.89) and one in a transonic working regime (M=1.03) [13].

The first cycle for the supersonic flow gave the values of forces and moments that define the aerodynamic coefficients and dimensionless coordinate of the center of pressure x_p. During the second cycle, under the same conditions, the fluid flow field around the models was visualized using the schlieren method.

In the transonic flow, the model with and without a spike was used to provide the forces and moments data. The duration of the cycles (air tunnel runs) was about 20 s and the angle of attack α took the values from 0° to 10°, with a step of 2°.

3.1 Results in the Supersonic Domain

During the supersonic regime in the tunnel, the mea–sured mean values of the properties for undisturbed flow and the properties calculated using Eqs. (1-5) were:
- in the silencing chamber, p_0 = 0.992 bar and T_0 = 278 K;

- in the test section, $p = 0.151$ bar, $T = 162$ K, $\rho = 0.324$ kg/m^3, $\mu = 1.1 \cdot 10^{-5}$ Pas, $p_d = 0.376$ bar, $u = 482.1$ m/s, $M = 1.89$ and $Re = 0.38 \cdot 10^6$.

Figures (4-9) show the influence of the four tested spikes on the aerodynamic characteristics of the model with a hemispheric nose. It can be seen that the axial force coefficient c_a, normal force coefficient c_n, drag force coefficient c_d, and lift force coefficient c_l increase with the angle of attack α for the model with all four tested spikes, as well as for the body without a spike. Differently from the previous work [10-12], coefficients c_d and c_l presented here take into account the correction in the base drag, caused by the mounting of the model on the tail sting support system.
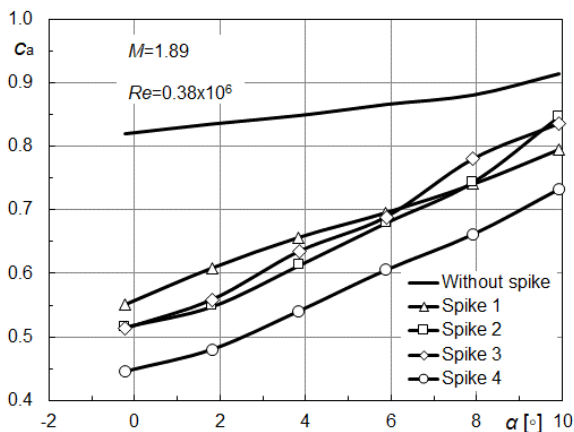

Figure 4. Axial force coefficient

With a spike on the tested model in supersonic airflow, regardless of its shape, a significant reduction of the axial and drag force coefficients occurs (Figs. 4 and 6). Moreover, an increase of the normal and lift force coefficients emerges (Figs. 5 and 7).
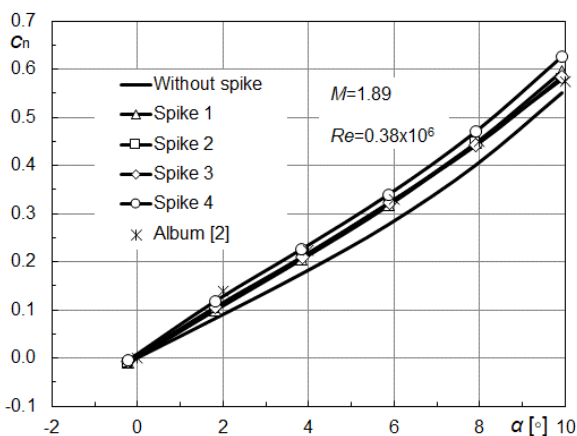

Figure 5. Normal force coefficient

The obtained results were compared with the results of Album and Hunt [2]. Album's results for the normal and lift force coefficients, for geometries and flow conditions similar to those presented here, are shown in Figures 5 and 7, respectively. Also, the results of Hunt, for the lift coefficient of a hemispheric body and spike with a conical tip at $M = 1.8$, are given in Figure 7. The agreement is quite good, especially for the tested model with spikes 1, 2, and 3, whereas our results for spike 4 are slightly better, for all angles of attack.
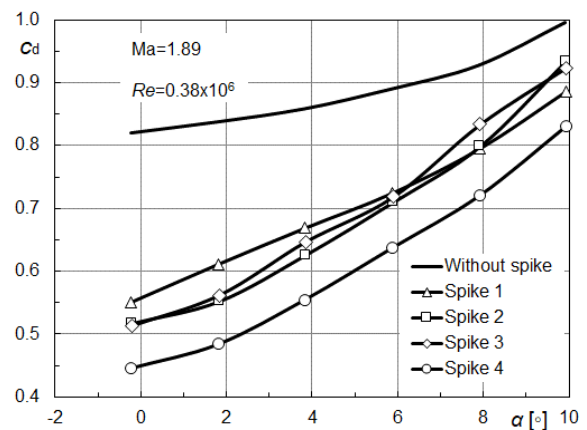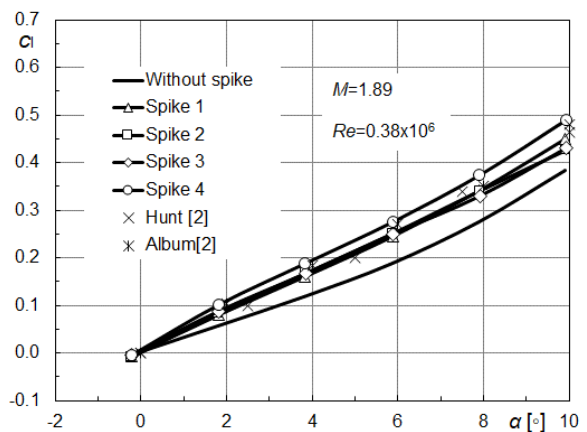

Figure 6. Drag force coefficient

Figure 7. Lift force coefficient

Figure 8 shows the decrement of pitching moment coefficient c_m with the angle of attack, for the body without and with all tested spikes. The presented value of the pitching moment coefficient corresponds to the moment at the tip of the model. All spikes lead to the reduction of the coefficient c_m.
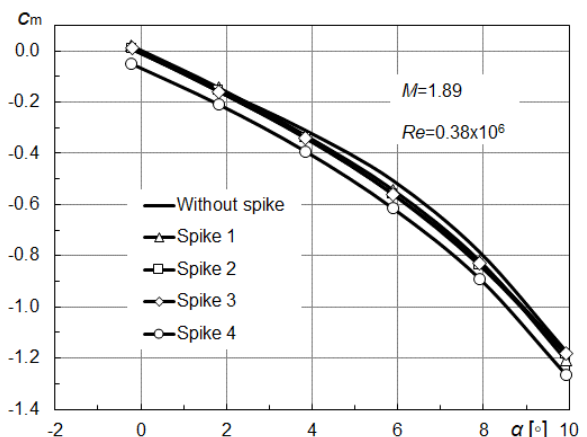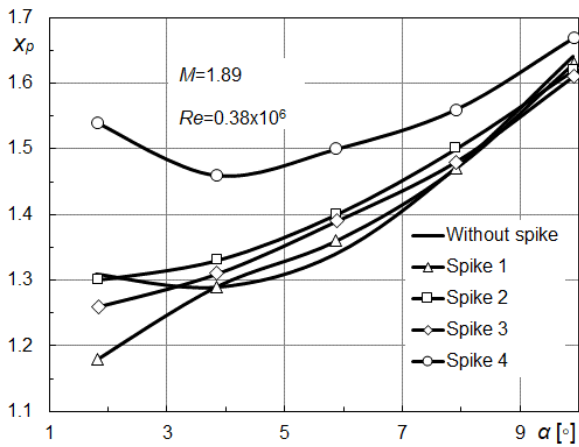

Figure 8. Pitching moment coefficient

The dimensionless coordinate of the center of pressure x_p is moved along the projectile axes backward with the angle of attack α, for all tested geometries when $\alpha \geq 4°$ (Figure 9). It is obvious that with mounting a spike the center of pressure moves towards the nose at α near to zero and about 10°, for the spikes 1, 2, and 3. The center of pressure moves the most downward for the model with spike 4, for all angles of attack. This improves the static stability of the body.

Figure 9. Dimensionless distance of the center of pressure from the tip of the hemispherical body

In conclusion, the tested model with the spike 4 (cylindrical with hemispheric tip) in supersonic airflow has the best aerodynamic characteristics, in the whole range of the angle of attack α. Among all four tested spikes, it is most effective for:

- reduction of the axial force coefficient,
- reduction of the drag force coefficient,
- reduction of the pitching moment coefficient,
- increment of the normal force coefficient,
- increment of the lift force coefficient, and
- moving the position of the pressure center backward, which is favorable from the aspect of the projectile stability.

The obtained relative decrease of the axial force Δc_a, the drag coefficient Δc_d, the pitching moment coefficient Δc_m, and the relative increase of the normal force Δc_n, the lift coefficient Δc_l, as well as the downward displacement of the dimensionless coordinate of the center of pressure Δx_p is systemized in Table 1. The calculated improvement Δy of an aerodynamic property of the model with the spike 4 (y_s), compared with the model without a spike (y), is calculated as:
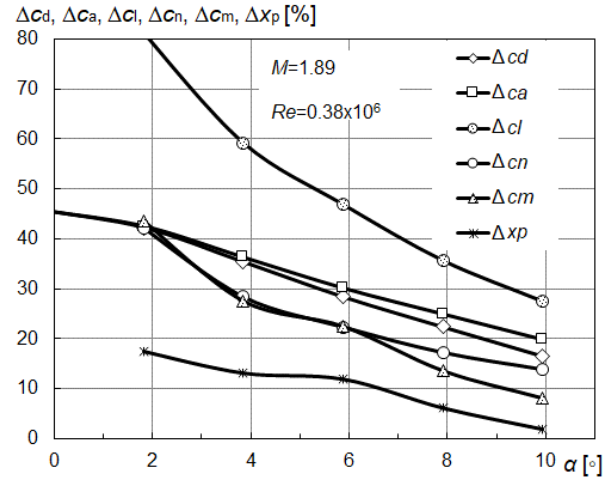
$$\Delta y = |y - y_s| / y . \qquad (9)$$

Table 1. The relative deviation of aerodynamic properties of the tested model with spike 4 from aerodynamic properties of the tested model without a spike
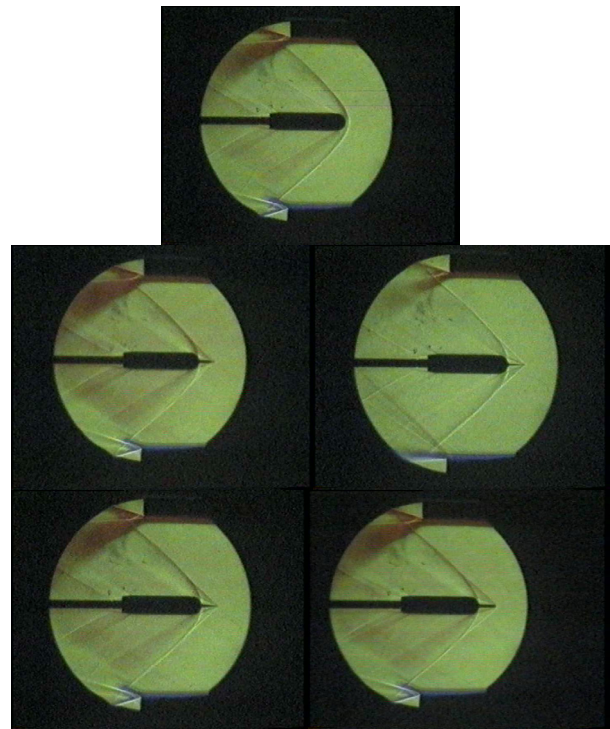
$\alpha[°]$	$\Delta c_a[\%]$	$\Delta c_n[\%]$	$\Delta c_d[\%]$	$\Delta c_l[\%]$	$\Delta c_m[\%]$	$\Delta x_p[\%]$
-0.23	46	/	46	/	/	/
1.80	42	42	42	81	44	18
3.83	36	28	35	59	28	13
5.86	30	22	28	47	23	12
7.90	25	17	22	36	14	6
9.91	20	14	17	28	8	2

The influence of spike 4 on the axial and drag forces is most notable for the zero angles of attack, reducing 46%. When the angle of attack increases to $\alpha \approx 10°$, relative reduction decreases to 20% for the axial and 17% for the drag force. The maximum influence of the spike 4 on the normal force coefficient's increase (42%), the lift coefficient's increase (81%), reduction of the pitching moment coefficient (44%), and movement of the center of pressure backward (18%) are obtained for the lowest tested value $\alpha \approx 2°$, while these influences

decrease with the increment of the angle of attack α. Figure 10 presents the decrement of the drag, axial, and pitching moment coefficients, the increment of the normal and lift coefficients, as well as the movement of the center of pressure downward, for the best-tested geometry (body with the spike 4), for all angles of attack.
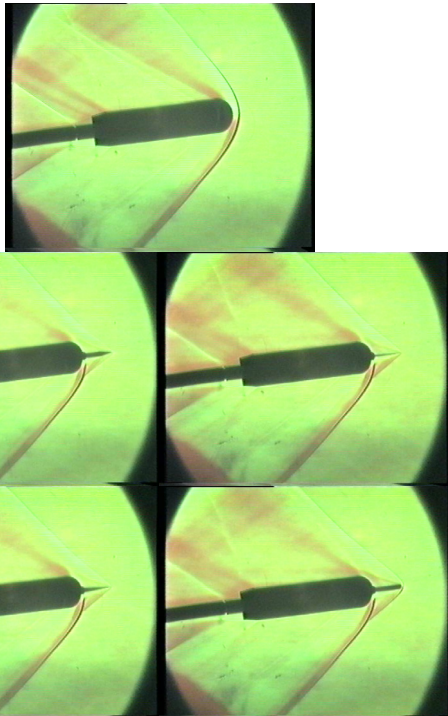

Figure 10. The improvement of the best-tested geometry (the model with the spike 4)

Figure 11. Schlieren photographs of the tested model without and with the spikes 1, 2, 3, and 4 for $\alpha \approx 0°$

All the above conclusions are following the photographs obtained by the schlieren technique. Figure 11 shows the photos of all tested models made with a video camera, which was used to check the occurrence of oscillations during the tests in the wind-tunnel T-36 at a near-to-zero angle of attack. A detailed examination of the recordings confirmed the absence of shock oscillations in any direction, which is by experiments of other authors for hemispheric tipped models with spikes [2, 3, 6, 9]. In addition, the presented flow patterns are similar to theirs.

A strong influence of a spike on the airflow field structure is evident. The semi-angle of the recirculation zone (due to the separation) for the model with all spikes is about 20 degrees (slightly smaller for spike 1 and slightly greater for spike 4). The angles of the conical shocks caused by the spikes correspond well to the angles of the conical shock waves that would be produced in the same supersonic flow past cone bodies whose angles are the same as the angles of recirculation zones shown in Figure 11 [10, 12, 13]. The strongest leading shock causes spike 4 with a rounded tip, compared with the others with conical tips. This implies the weakest following shock wave at the shoulders of the model with spike 4, compared to the cases with the model with conical spikes. Thus, the pressure increase through that second shock wave is smaller, and thus the model with spike 4 is the best among all tested. That implies a smaller total loss of mechanical energy, which is consistent with the results of the aerodynamic coefficients.

Figure 12. Schlieren photographs of the tested model without and with the spikes 1, 2, 3, and 4 for $\alpha \approx 6°$

Figure 12 shows the schlieren photographs of the tested model without and with the spikes 1, 2, 3, and 4, respectively, at the angle of attack $\alpha \approx 6°$. The flow pattern is not axisymmetric anymore. The differences among the tested spikes diminish for superior angles of attack, which corresponds well to the results of the above presented aerodynamic coefficients. The strongest leading conical shock wave followed by the weakest one, still appears on the model with spike 4, making it the best choice among tested, for an angle of attack higher than zero.

3.2 Results in the Transonic Domain

A set of measurements was performed to obtain the forces and moments data in the transonic area also, for the model without and with all four spikes. During the tests in wind tunnel T-36, the measured mean values of the properties for an undisturbed flow and the properties were calculated using Eqs. (1-5) were:

-in the silencing chamber, $p_0 = 1.008$ bar and $T_0 = 278.5$ K;

-in the test section, $p = 0.522$ bar, $T = 230.8$ K, $\rho = 0.788$ kg/m^3, $\mu = 1.5 \cdot 10^{-5}$ Pas , $p_d = 0.387$ bar,

$u = 313.6$ m/s, $M = 1.03$ and $Re = 0.44 \cdot 10^6$.

The results showed that there is no effect of any spike, regardless of its shape. Moreover, the measurements of the aerodynamic load of the tested model gave even worse results for the model with a spike compared with the model without it.

Table 2. The drag and lift coefficients of the tested model with spike 4 and its relative deviation from the tested model without a spike

α	c_d	c_{d4}	$\Delta c_{d4}[\%]$	c_l	c_{l4}	$\Delta c_{l4}[\%]$
-0.2	0.3887	0.3871	0.4	/	/	/
1.8	0.3897	0.3949	1.3	0.0518	0.0506	2.3
3.9	0.4022	0.4078	1.4	0.0989	0.0995	0.6
5.9	0.4283	0.4342	1.4	0.1518	0.1502	1.1
7.9	0.4716	0.4786	1.5	0.2092	0.2092	0.0
9.9	0.5192	0.5351	3.1	0.2941	0.2771	5.8

Table 2 shows the results of the drag and lift coefficients for the models without and with the spike 4 for $M = 1.03$ and $Re = 0.44 \cdot 10^6$. The presented results approve that the spike does not improve the aerodynamic characteristics of the tested hemispheric model in the transonic area, as opposed to its important role in the supersonic area.

4. CONCLUSION

The paper has treated experimentally the influence of a spike and its shape on the supersonic and transonic flights of a hemispheric projectile. The experiments were performed in VTI's small trisonic wind tunnel T-36, with Mach numbers $M_\infty = 1.89$ and $M = 1.03$, for the model without and with four different spikes. The length of the spikes was equal to the body diameter and the angle of attack varied from 0° to 10°. The measurements took into account the correction in the base drag caused by the connection between the tested model and the tail sting support system.

It turned out that all tested spikes improve the aerodynamic characteristics only in the supersonic domain. In particular, the cylindrical spike with a hemispheric tip performed the best in terms of all examined aerodynamic parameters. This spike caused a 46% drag reduction at a near-to-zero angle of attack and an 81% lift increment at $\alpha \approx 2°$. As opposed to supersonic, the experiments in the transonic domain confirmed that the spikes do not affect aerodynamic properties, regardless of their shape.

These measurements were completed by the visualization in the supersonic domain, which was performed in the same wind tunnel by the schlieren method. The rounded tip of spike 4 caused the strongest leading shock wave followed by the weakest one, compared with the other tested spikes. This weakest second wave implied the smallest pressure increase

behind the shock and consequently caused the smallest drag, as well as the best other aerodynamic coefficients for the model with spike 4. Finally, the measurements are validated by the results of other authors, and a good agreement has been achieved.

Results of this kind of experiment, which are always very demanding and expensive, are always precious. The results presented here may serve as a benchmark for numerical solutions to similar problems. Moreover, the conclusions from the measurements, as well as the visualized flow around the tested models, may have wide applications. In future studies, they can serve for a preliminary selection of an appropriate shape of the spike, before experimental or numerical analyses that would provide the best flight conditions of projectiles or aircrafts moving supersonically.

ACKNOWLEDGMENT

REFERENCES

[1] Chang, P.K.: *Control of Flow Separation: Energy Conservation, Operational Efficiency, and Safety*, Hemisphere Publish. Corporation, Washington, 1976.

[2] Chang, P.K., "Flow Separation on Thin Protruding Probes Placed in Front of Blunt Bodies at Supersonic/Hypersonic Speeds," *Separation of Flow*, 1st ed., Pergamon Press, pp. 469-530, 1970.

[3] Krasnov, N.F. et al.: "Drag and Lift Control," *Control and stabilization in aerodynamics* (in Russian), High school, Moscow, pp. 383-394, 1978.

[4] Ahmed, M.Y.M., Qin, N.: Forebody shock control devices for drag and aero-heating reduction: A comprehensive survey with a practical perspective, *Progress of Aerospace Sciences*, Vol. 112, 100585, January 2020.

[5] Huang, W. et al.: Drag and heat flux reduction mechanism induced by the spike and its combinations in supersonic flows: A review, *Progress in Aerospace Sciences*, Vol. 105, 31-39, 2019.

[6] Mair, W. A.: Experiments on Separation of Boundary Layers on Probes in Front of Blunt-Nosed Bodies in a Supersonic Air Stream, *Phil. Mag.*, Ser.7, Vol.43, No.342, pp.695-716, July 1952.

[7] Hahn, M.: Pressure Distribution and Mass Injection effects in the Transitional Separated Flow over a Spiked Body at Supersonic speed, *J. Fluid Mech.*, Vol. 24, Part 2, pp. 209-223, 1966.

[8] Bogdonoff, S. M., Vas, I. E.: "Preliminary Investigations of Spiked Bodies at Hypersonic Speeds," *J. Aero/Space Sciences*, Vol. 26, No. 2, February 1959, pp. 65-74.

[9] Calarese, W., Hankey, W. L.: "Modes of Shock-Wave Oscillations on Spike-Tipped Bodies," *AIAA Journal*, Volume 23, No.2, February 1985, pp.185-192.

[10] Milićev, S.S., Pavlović, M.D., Vitić, A., Ristić, S.: Experimental study of the Influence of Spike Shape at Supersonic Axisymmetric Flow Past Bodies, *Proceedings of the 23rd Yugoslav Congress of Theoret. And Applied Mechanics*, 261-264, Belgrade, 2001.

[11] Milićev, S.S., Pavlović, M.D., Ristić, S., Vitić, A.: On the influence of spike shape at supersonic flow past blunt bodies, *Facta Univ. – Ser. Mech. Automatic Control Rob. 3*, 371-382, 2002.

[12] Milicev, S. S., Pavlovic, D. M.: Influence of Spike Shape at Supersonic Flow Past Blunt Nosed Bodies: Experimental Study, *AIAA Journal*, Vol. 40, issue 5, 1018–1020, 2002.

[13] Milićev, S. S.: *Supersonic Flow around Blunt Bodies of Revolution with Spike*, (in Serbian), M. Sc. Thesis, University of Belgrade, Faculty of Mechanical Engineering, Belgrade, 1999.

[14] Sahoo D., Das S., Kumar P., Prasad J.: Effect of spike on steady and unsteady flow over a blunt body at supersonic speed, *Acta Astronautica*, Vol. 128, pp. 521–533, 2016.

[15] Tembhurnikar, P. V., Akash T. J., Sahoo D.: Effect of Intermediate Aerodisk Mounted Sharp Tip Spike on the Drag Reduction over a Hemispherical Body at Mach 2.0, *FME Transactions*, Vol. 48, No 4, pp. 779-786, 2020.

[16] Ahmed, M.Y.M., Qin, N.: Drag reduction using aerodisks for hypersonic hemispherical bodies, *Journal of Spacecraft Rockets*, Vol. 47 (1), 62-80, 2010.

[17] Yadav, R. et al.: Aerothermodynamics of a hypersonic projectile with a double-disk aerospike, *Aeronautical Journal*, Vol. 117, no. 1195, 913–928, 2013.

[18] Milićev, S.S., Ćoćić, A.S.: *Compressible Fluid Flow Calculation Handbook with the Theory Excerpts*, (in Serbian), University of Belgrade, Faculty of Mechanical Engineering, Belgrade, 2017.

[19] Ocokoljić, G., Damljanović, D., Rašuo, B., Isako–vić, J.: Testing of a standard model in the VTI's large-subsonic wind-tunnel facility to establish users' confidence, *FME Transactions*, 42 (3), pp. 212-217, 2014.

[20] Damljanović, D., Vuković, Dj., Ocokoljić, G., Rašuo, B.: Convergence of transonic wind tunnel test results of the AGARD-B standard model, *FME Transactions*, Vol. 48, No. 4, pp. 761-769, 2020.

[21] Damljanović, D., Vuković, Đ., Ocokoljić, G., Ilić B, Rašuo, B.: Wind Tunnel Testing of ONERA-M, AGARD-B and HB-2 Standard Models at Off-De–sign Conditions, *Aerospace*, Vol. 8 (10), 275, 2021.

ЕКСПЕРИМЕНТАЛНА СТУДИЈА О УТИЦАЈУ ИГЛЕ НА НАДЗВУЧНО И ОКОЛОЗВУЧНО ОПСТРУЈАВАЊЕ ТЕЛА ПОЛУСФЕРНОГ ВРХА

С. Милићев

Снажан ударни талас, који настаје при надзвучном лету пројектила заобљеног врха, значајно повећава његов отпор и аеродинамичко загревање. Оба ефекта могу да се умање монтирањем игле на врх пројектила. Осим постојања саме игле, и њена дужина и облик такође могу да утичу на аероди–намичке карактеристике заобљеног тела. Овај рад приказује експерименталне резултате утицаја облика игле на аеродинамичке коефицијенте сила и момената, као и на позицију центра притиска, при надзвучном и околозвучном опструјавању модела пројектила полусферног врха. Експеримент је изведен у трисоничном аеротунелу при Маховим бројевима $M=1,89$ и $M=1,03$ и различитим нападним угловима ($0°$-$10°$). Визуализација струјног поља при надзвучном опструјавању модела изведена је шлирен методом. Она је омогућила квалитативну анализу струјног поља ваздуха око модела без игле и модела са четири игле различитог облика. На основу визуализације струјног поља изведени су закључци који су у складу са добијеним бројним вредностима аеродинамичких коефицијената. Експерименти показују да игла и њен облик имају утицаја само при надзвучном лету пројектила, док игла не утиче, или чак мало погоршава аеродинамичке карактеристике пројектила при околозвучном лету. Добијени резултати се могу шире применити, на пример при пројектовању суперсоничних летилица.